ELSEVIER

Materials Characterization 53 (2004) 17–28

MATERIALS CHARACTERIZATION

High strain gradient measurements by using digital image correlation technique

Fabienne Lagattu*, Jean Brillaud, Marie-Christine Lafarie-Frenot

Laboratoire de Mécanique et de Physique des Matériaux, UMR CNRS, ENSMA-Site du Futuroscope, BP40109, 86961 Futuroscope, France

Received 28 April 2004; received in revised form 27 June 2004; accepted 27 July 2004

Abstract

When material characterization requires nonhomogeneous strain field measurements, the use of specific techniques is necessary. In this paper, the efficiency of the digital image correlation method for measuring in-plane displacements in the presence of high strain gradient is discussed. Three types of strain gradient have been studied: strain localization around a hole in a composite laminate, strain concentration at a crack tip in a TiAl alloy, and strain gradient on a polymer neck front. These three applications concern various materials, various types of loading, and various gradient values. Results demonstrate the technique capabilities for a wide range of cases.

Keywords: Strain concentration; Correlation; Material behaviors

1. Introduction

Engineering and structure design require knowledge of material constitutive laws. In the case of nonhomogeneous strain distribution, material characterization needs the use of specific techniques of measurement. In that field, optical whole-field techniques are of great interest. Photoelasticimetry gives the state of stress in the specimen [1,2]. But this method requires a birefringent material, which is stuck on the studied sample or which replaces the actual prototype. The moiré method needs to print gratings on the surface of the test specimen. It can be used in several experimental configurations [3–5]. But spatial resolution and experimental difficulties with this method are directly linked with the grid step. Holographic technique is also attractive because of its high sensitivity [6] but it needs an extreme environmental stability. The efficiency of one or another method depends on the measurement requirements. The goal of our study is to obtain quite rapidly and easily « in situ » displacement measurements, that is to say on the mechanical testing machine, with a good accuracy and a good

* Corresponding author. Tel.: +33 5 49 49 82 28; fax: +33 5 49 49 82 38.

E-mail address: lmpm@lmpm.ensma.fr (F. Lagattu).

1044-5803/$ - see front matter © 2004 Elsevier Inc. All rights reserved.
doi:10.1016/j.matchar.2004.07.009

spatial resolution. Thus, we have chosen to apply 'speckle' methods.

Laser speckle method has been described and used by many authors [7–10]. In our laboratory, we have also applied it in various configurations [11]. However, a severe drawback of this technique remains: the abrupt speckle decorrelation in the presence of out-of-plane displacement, light source variation, or excessive deformation of the object. Thus, using recent progress in digital cameras, we have used the white light speckle method (also called digital image correlation) [12].

Several authors have used and enhanced the capabilities of this technique, which is particularly adapted for studying strain heterogeneities [13–18]. But its spatial resolution is usually larger than 1 mm [13–17], which is not appropriate for studying very high strain gradients, or, when the spatial resolution is thinner, the studied zone is reduced to 2.5 mm^2 [18].

The aim of this paper is to discuss the efficiency of the digital image correlation procedure that has been developed in our laboratory for measuring in-plane displacements on material surface in the presence of high strain gradient, with a thin spatial resolution. Three types of strain gradient have been studied: strain localization around a hole in a composite laminate, strain concentration at a crack tip in a TiAl alloy, and strain gradient on a polymer neck front. These three applications concern various materials, various types of loading, and various gradient values. It allows testing the technique capabilities for a wide range of cases.

In the first part, the white light image correlation technique is described. Then, experimental results obtained in the three different cases of strain gradient are presented. Finally, limits and performances of the method for strain gradient measurement are discussed.

2. Experimental procedure

The white light image correlation method can be divided into three steps: the specimen preparation, the data acquisition, and the data analysis. For each step, we have developed a specific procedure in order to optimize the final experimental performances.

2.1. Specimen preparation

The aim is to create a random grainy aspect of the specimen surface. The smaller the grains, the higher the spatial resolution. Moreover, the grain diameters must be as regular as possible. On the other hand, in order to follow the material deformation during the test, the grains have to be well fixed on the surface and to remain adherent, whatever the specimen material and the loading conditions are. However, the grain coating must not disturb the strain field of the sample. Therefore, we have perfected a special mixture containing very fine white and black powders [12], which is sprayed on the sample surface. The result consists in a white and black random grain field, the highest spatial frequency of which corresponds to dimensions of about 30 μm. The limit of adhesion or destruction of this special mixture depends on the studied material. We have experimentally observed that this mixture remains adherent to the surface of polymer specimens up to strain values superior to 50%. On composite material surface, the apparition of large cracks on the specimen surface during tests can remove the mixture around these cracks, and create zones where displacement measurements are no longer possible. On metallic material, we have observed that after 30,000 cycles of fatigue loading at 20 Hz, the grainy pattern is not deteriorated, even at the crack tip. Hence, these various tests demonstrate that the use of this mixture allows a wide range of studies.

2.2. Data acquisition

To take digital photography of the grain field, the object surface is illuminated with a fluorescent tube. An optical and mechanical assembly was designed and mounted on the testing machine. With this assembly, the support of the digital camera is connected to the testing machine jaws by elastic suspensions, to limit the general displacement between two consecutive pictures. A standard digital camera with a focal length of 21 mm and a CCD matrix containing more than 6 million pixels (3008×2000 pixels with 256 grey levels) is used. The distance between the camera and the specimen is about 75 mm, which allows to neglect the influence of out-of-plane displacements on in-plane measure-

ments. The focus distance is adjusted by using a micrometer translator. Pictures are recorded with a magnification of about 1/2. In this experimental configuration, one pixel of the CCD matrix corresponds to an area of about 9×9 μm on the object. Thus, one grain, which has an average diameter of 30 μm, is defined by about 3×3 pixels on the CCD matrix. Because we use standard optical lens, the extreme corners of the recorded picture are disturbed by optical aberrations. Thus, these zones have not been explored during experiments.

2.3. Data analysis

The principle used for measuring the whole-field displacements of the specimen surface has been first proposed by Burch and Tokarski [19]. The unique pattern of random grains is recorded twice, once before loading the sample, and the other when the sample is deformed (Fig. 1). Displacement vectors are determined by comparing the two pictures. The first picture is divided into small subwindows. The discrete matrix of the values of the pixel grey level in each subwindow forms a unique fingerprint identification within the image. Therefore, at every 'point', i.e., at every subwindow center, it is possible to determine the in-plane displacement vector.

The computer software, GRANU.EXE, which has been developed in our laboratory [12], is based on the calculation of the direct correlation of two subwindow matrices. This software has been written in the C++ programming language, and needs as inputs:

- coordinates (x_k,y_k) of points G_k where the displacement values are calculated;
- size N of the square subwindow;
- correlation threshold value.

To calculate the displacement value at the chosen point G_k, a subwindow of the given size centered at G_k is 'cut out' from the first picture. It is noted subwindow 1 in Fig. 2. Then, the software calculates the correlation value of this subwindow with a subwindow of the same size, taken in the second picture, and centered at a point P_i (Fig. 2). This point P_i is randomly chosen in the second picture, near the corresponding point G_k. The calculated correlation value is the normalized pixel by pixel multiplication of the two subwindows (noted SW_1 and SW_2), given by Eq. (1):

$$C_{G_k}(P_i) = \frac{\mathcal{C}_c(SW_1(G_k),SW_2(P_i))}{\sqrt{\mathcal{C}_s(SW_1(G_k))}\sqrt{\mathcal{C}_s(SW_2(P_i))}} \quad (1)$$

where $\mathcal{C}_c$ et $\mathcal{C}_s$ are, respectively, the cross-correlation and self-correlation functions. These functions are

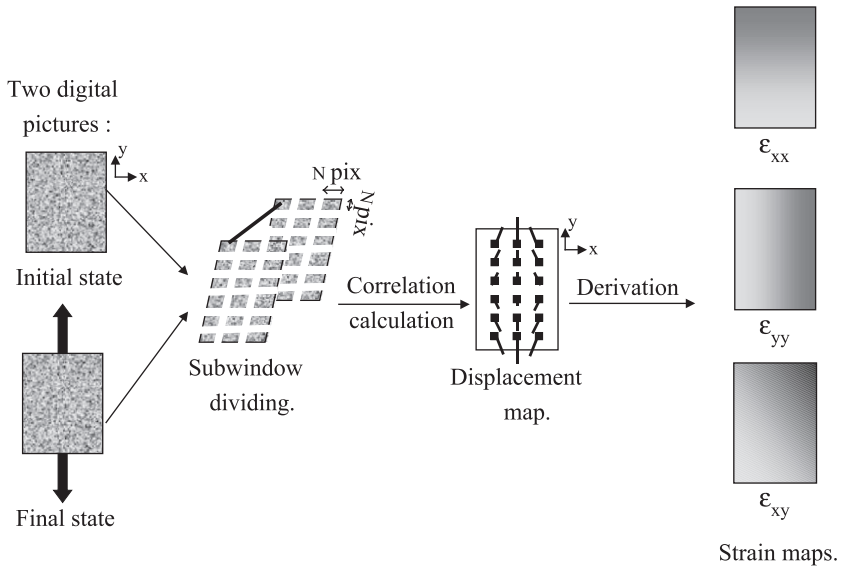

Fig. 1. Principle of digital image correlation method used for in-plane strain mapping.

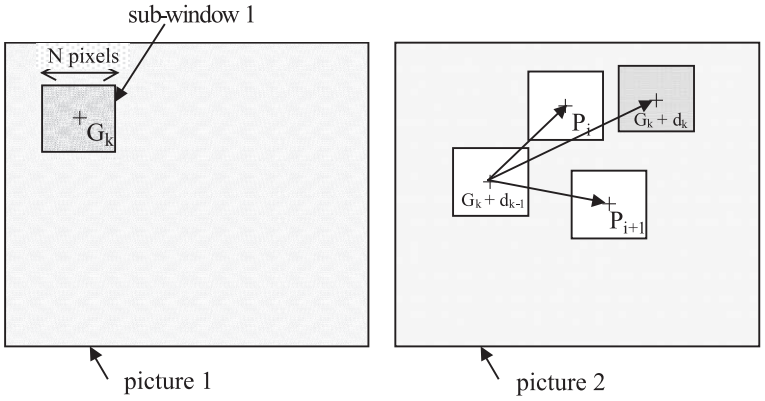

Fig. 2. Schematic representation of the different steps executed by the GRANU.EXE software.

defined by Eqs. (2) and (3), where I represents the pixel intensity level:

$$\mathcal{C}_c(\mathrm{SW}_1(G_k),\mathrm{SW}_2(P_i)) = \sum_{i=-\frac{N}{2}}^{\frac{N}{2}} \sum_{j=-\frac{N}{2}}^{\frac{N}{2}} I_{\mathrm{SW}_1}(x_k+i, y_k+j) \cdot I_{\mathrm{SW}_2}(x_k+i+u_{P_i}, y_k+j+v_{P_i}) \quad (2)$$

$$\mathcal{C}_s(\mathrm{SW}_1(G_k)) = \frac{1}{N^2} \sum_{i=-\frac{N}{2}}^{\frac{N}{2}} \sum_{j=-\frac{N}{2}}^{\frac{N}{2}} I_{\mathrm{SW}_1}(x_k+i, y_k+j) \cdot I_{\mathrm{SW}_1}(x_k+i, y_k+j) \quad (3)$$

where (u_{P_i}, v_{P_i}) are the components of the displacement vector from G_k to P_i.

If the calculated correlation value at the point P_i is less than the one corresponding to the threshold value, the program will go to the next randomly chosen point P_{i+1}. If it is higher, the program will execute systematic calculations of correlation values in a region of 7×7 pixels^2 around P_i, in order to obtain the shape of the correlation function in this region. Different numerical tests are then performed on the correlation peak to detect if it corresponds to an erratic point. At first, the correlation values around the peak maximum are compared with the value corresponding to the given threshold. The correlation threshold value is determined as a percentage of the difference between the maximum correlation value and the noise level. When using pictures with good white and black contrast and small strain values, the threshold value can reach up to 35%. For noisy pictures and/or for high strain values, it can decrease to 20%. The user has to choose a good compromise between a too small threshold value that would give values at every point, even erratic points, and a too high threshold value that would lead to consider all the points as erratic ones. Generally, the threshold value is chosen by testing three or four values between the two first pictures, and then this value is applied to every couple of pictures of the same set. Other numerical tests performed on the correlation peak concern its shape: the software checks the correspondences between a biparabolic peak and the experimentally obtained peak.

If it is detected that the considered point corresponds to an erratic point, another try is done to correlate subwindow 1 with another subwindow centered at a neighboring point of P_i. On the contrary, if the tested point is correct, a biparabolic least-square fitting is performed and the displacement value d_k of the point G_k is calculated as being the vector from G_k to P_i, given by its two components (u_k,v_k).

In order to determine the displacement value at G_{k+1}, the software starts its research with a subwindow in the second picture shifted by the previous computed displacement value d_k. It allows to reduce the time of searching the new localization of subwindow 1 in picture 2. When this shift value is unknown, the searching is also efficient but more time consuming.

When the complete displacement field is obtained, the data file is automatically transferred to a finite element code. The FEM software is used to derive the experimental data in order to obtain the in-plane strain values. Each point G_k becomes a node of the

finite element mesh, and the measured displacement vectors are imposed as boundary conditions. Visualization facilities of the FEM software are used to present strain maps.

The GRANU.EXE software is able to determine displacement values for 1000 'points' on the sample surface in 15 s, using a standard 1.2-GHz PC. With the chosen magnification, the total studied area is about 20×20 mm. Because of the very fine grainy pattern that was deposited on the specimen surface, we obtain an interesting spatial resolution: one subwindow covers an area of about 300×300 μm^2.

An example of a correlation peak experimentally obtained is presented in Fig. 3. The calculation has been performed in a region of 7×7 pixels^2 around the correlation peak crest, for a strain value of 2%, with a subwindow size of 30×30 pixels^2. Experimental data are compared with parabolic fitting along the two medium axes (Fig. 3a and b). One can see that the use of a biparabolic fitting for locating the maximum of the correlation peak is suitable. As we have shown in a previous study [12], the correlation peak flattens when the strain value increases. It leads to difficulties in determining the location of the peak maximum value, that is, the displacement value. Thus, the measurement accuracy decreases when the strain value increases. Calibration tests with a tensile–flexural device have allowed to determine the dispersion of displacement measurement versus strain values (Fig. 4). Thanks to the biparabolic fitting, we obtain subpixel accuracy. One can see in Fig. 4 that the dispersion of displacement measurement varies from 4×10^{-2} to 23×10^{-2} pixels. This means that in the usual measured strain range, the average accuracy of the displacement values is approximately 1/10 pixel, i.e., approximately 1 μm. But for strain values about 8%, this accuracy becomes 2 μm.

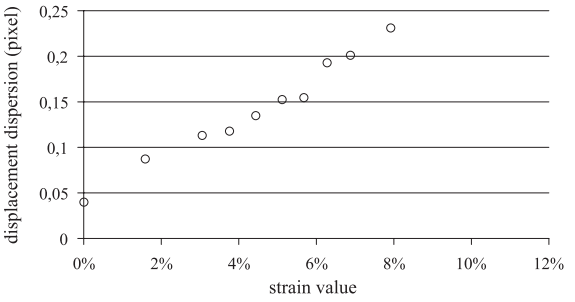

Fig. 4. The dispersion of displacement measurement versus strain values.

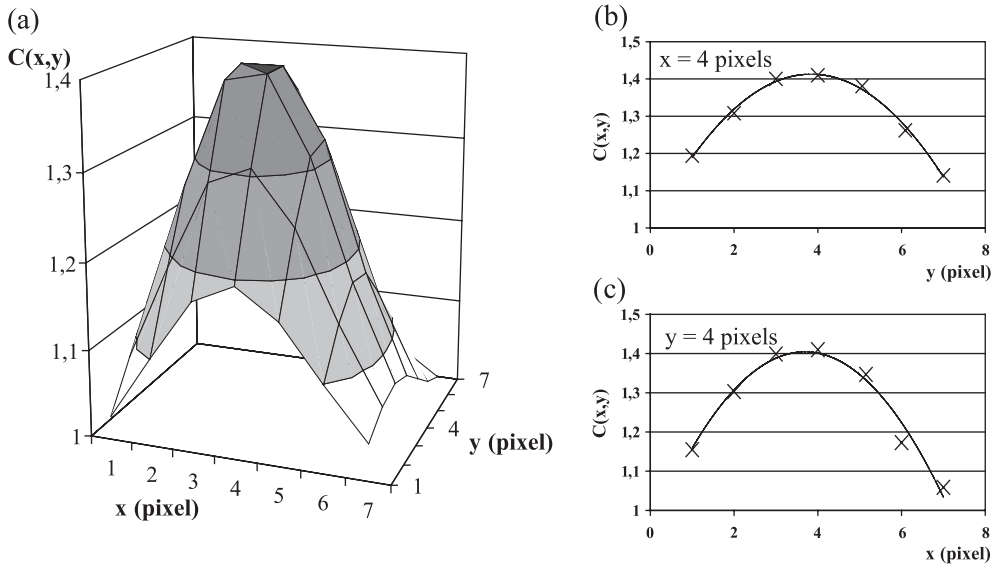

Fig. 3. Example of a correlation peak experimentally obtained for a strain value of 2%: the calculation has been performed in a region of 7×7 pixels^2 around the correlation peak crest, with a subwindow size of 30×30 pixels^2. (a): View in perspective, (b) x=4 pixels section plot and parabolic fitting, (c) y=4 pixels section plot and parabolic fitting.

3. Strain localization around a hole in a composite laminate

3.1. Experimental conditions

The understanding of notched composite specimen behavior becomes necessary for complex structure design [20]. In a previous study, it has been shown that the notched specimen strength is directly linked to the different types of damage occurring around the hole [21]. In order to characterize and quantify overstrain accommodation which develops near the notch, we have used the white light image correlation technique [22]. The studied composite laminate has long carbon fibers as reinforcements and a thermoplastic matrix. Specimen geometry is given in Fig. 5, with the x-axis as the loading axis. Tensile specimens have two 5-mm-diameter holes, and compressive ones are shorter with only one hole. Tensile and compressive tests with several loadings/unloadings have been performed at room temperature, with a constant crosshead displacement rate of 0.1 mm/min. The grainy pattern images around the hole have been recorded at different stress levels, up to the failure of the specimen. Displacement values have been measured near the hole in 504 'points', distributed on a

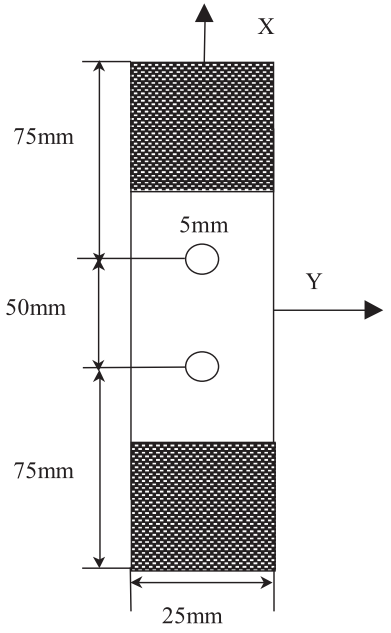

Fig. 5. Notched composite laminate specimen geometry.

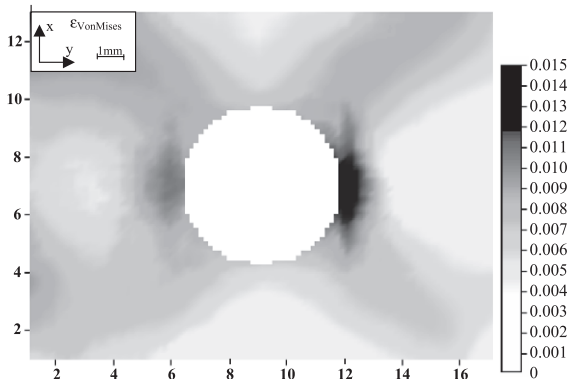

Fig. 6. Von Mises strain map measured by digital image correlation technique around the hole of 5 mm diameter on a thermoplastic matrix composite, $\sigma_{applied}$=67% $\sigma_{failure}$.

16×12 mm area of the specimen surface. The nearest 'point' from the hole is located at about 200 μm from the notch edge. The mesh has been constructed in order to fit with the local gradient of the expected strain distribution. Therefore, near the hole, the distance between two 'points' is equal to 145 μm, and increases up to 435 μm far from the hole.

3.2. Results

Fig. 6 presents the Von Mises strain map measured on the notched composite specimen at a tensile stress of 67% of the failure strength. The correlation calculations have been performed between the initial picture of the virgin specimen recorded before any loading, and the picture taken when the specimen was loaded at 67% of the ultimate stress. One can see in this figure that the highest strain values are localized on the y-axis, close to the hole. Four zones of high strains (ε_{VM}~0.9%) are developed along the $\pm 45^{\circ}$ axes, in a quasi-symmetrical way.

In order to compare the strain distribution according to the applied stress, we have plotted Fig. 7 longitudinal strain values measured along the y-axis of the net section, in the vicinity of the hole. Fig. 7 presents experimental data obtained for three loading levels in tension and in compression. For compressive tests, by comparing experimental data with linear elastic calculation, it has been shown that the notched composite specimen behavior corresponds to that of a linear elastic material, up to failure [22]. But, in tension, for tensile loads higher than 50% of the

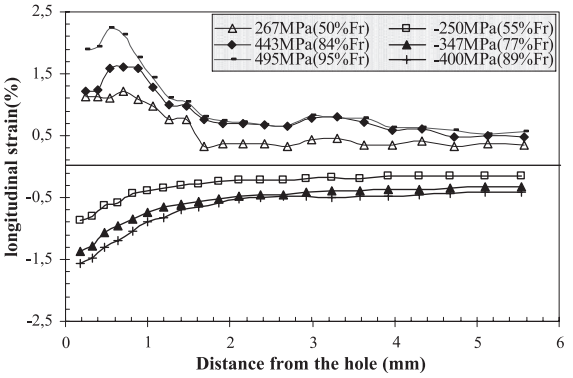

Fig. 7. Tensile and compressive tests on a notched composite laminate: longitudinal strains measured by digital image correlation method on the y-axis of the net section for different values of the applied stress.

failure stress, an overstrain peak appears at a distance of about 700 μm from the hole. The higher the applied load, the greater the maximum strain value. One can see in Fig. 7 that, for an applied stress of 95% of the failure stress, strain values varies from 0.6% to 2.3% in a localized 1.1-mm-long region, corresponding to a strain gradient value of 1.54×10^{-2} mm^{-1}. These measurements show that the accuracy and spatial resolution of the used digital image correlation technique allows a quantitative description of strain values in presence of such a gradient.

4. Strain concentration at a crack tip in a TiAl alloy

4.1. Experimental conditions

It has been shown that fatigue crack growth resistance of TiAl alloy depends strongly on its microstructure [23]. In order to get insights into the crack propagation mechanisms in TiAl alloy, full-field in-plane strains were measured by digital image correlation technique near a fatigue crack tip [24].

Fig. 8 presents the experimental conditions of this study. The used sample is a standard Compact Tension specimen, the dimensions of which are given in Fig. 8a. A fine grainy pattern has been sprayed on the specimen surface (Fig. 8b). The sample has been submitted to a fatigue loading, from F_{min}=285 N to F_{max}=2849 N. After 30,000 cycles of fatigue loading at 20 Hz, the crack has propagated from a_0=0.5 mm to a=1.03 mm, with ΔK=7.5 MPa $m^{1/2}$. We present here the measurements of the residual strains created by each cycle of fatigue loading. The first picture is taken at the minimum load of a cycle (F_{min}, corresponding to K_{min}=0.832 MPa $m^{1/2}$), then the sample is subjected to a loading cycle, and the second picture is taken at the next F_{min}. In-plane displacements are measured at mesh nodes shown in Fig. 9. Two meshes have been tested in order to highlight the influence of the chosen mesh. Each mesh covers a total area of 12×12 mm. Thanks to the high spatial resolution of the applied technique, in the two meshes, the nearest 'point' to the crack is located at 135 μm of the crack tip. In mesh 1 (Fig. 9a), there are 415 'points' of measurement, and the distance between two 'points' varies from 100 μm at the crack tip to 1500 μm far from the crack tip. Mesh 2 is finer (Fig. 9c), with 1265 'points' of measurement, separated by 30 μm at the crack tip and 280 μm far from the crack tip.

4.2. Results

The measured residual strain maps are presented in Fig. 9b for mesh 1 and in Fig. 9d for mesh 2. Experimental maps are roughly the same. In the two cases, the Von Mises strain distribution shows a high overstrain localization at the crack tip, whereas strain values in the rest of the specimen remain negligible. It demonstrates a plastic strain accumulation around the crack tip, after each cycle of loading. The comparison of the two different mesh results shows that the finer the mesh, the noisier the measurements. It is due to the fact that for a given displacement measurement accuracy, when points are closer, strain accuracy is worse. That is why, for each type of test, the user has to

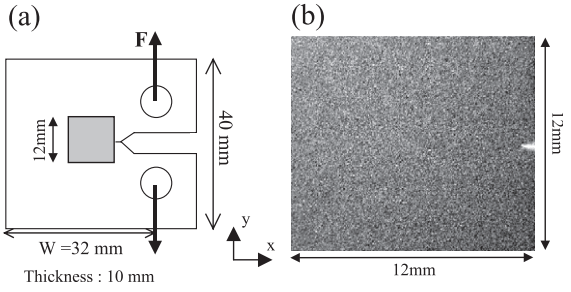

Fig. 8. (a) Specimen geometry, (b) grainy pattern image.

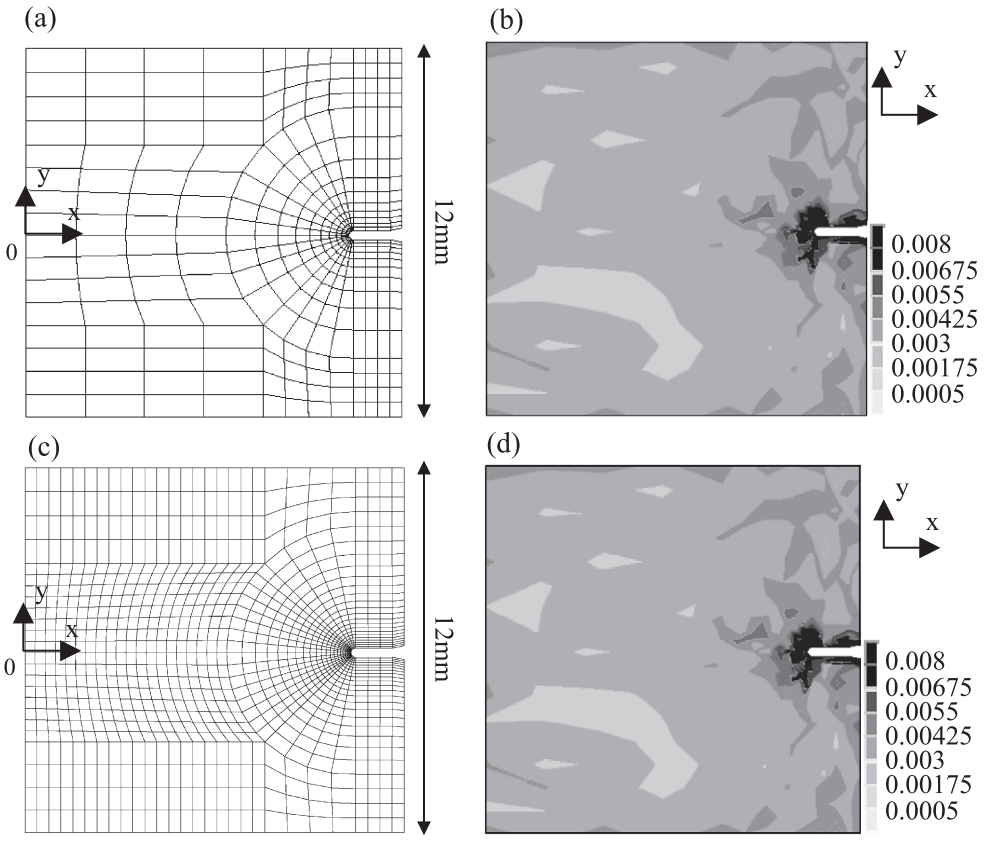

Fig. 9. Residual strains created by a fatigue cycle on the TiAl alloy: (a) points of measurement in mesh 1, (b) experimental Von Mises strain map obtained with mesh 1, (c) points of measurement in mesh 2, (d) experimental Von Mises strain map obtained with mesh 2.

choose the appropriate mesh, in relationship with the required method accuracy and the expected strain gradient. Fig. 10 are plotted ε_{yy} strain evolutions along the x-axis, ahead of the crack tip for the two meshes. As the x-axis origin has been taken at the left extremity, the crack tip location is x=9.5 mm (Fig. 9a and c). One can see in Fig. 10 that for the two meshes, strain evolutions are globally the same. But, as we have seen in strain maps, measured values are noisier with the finer mesh (mesh 2). Fig. 10 shows that, for the two meshes, the residual strains are concentrated very close to the crack tip. On a 1-mm-long distance, strain values vary from 1.6% to −0.4%, corresponding to a strain gradient value of 2.0×10^{-2} mm^{-1}. With mesh 1, which is the more appropriate in this study, the dispersion around zero of the measured strain values far from the crack tip gives a typical error of 5×10^{-4}.

5. Strain gradient on a polymer neck front

5.1. Experimental conditions

Neck propagation in polycarbonate (PC) tension specimen is a well-known phenomenon. This type of glassy polymers presents a well-defined yield point, which is followed by a sharp drop of the stress in conventional stress–strain diagrams. This drop is accompanied by the initiation of a neck, which propagates across the whole length of the specimen. It is difficult to obtain quantitative data to characterize the postyield behavior, because strains are very large and nonhomogeneous. For example, the neck initiation has been studied by Bauwens-Crowet et al. [25], using photoelasticimetry. Theocaris and Hadjiiossiph [26] have obtained strain maps on polycarbonate specimen by using the moiré technique. Nied and

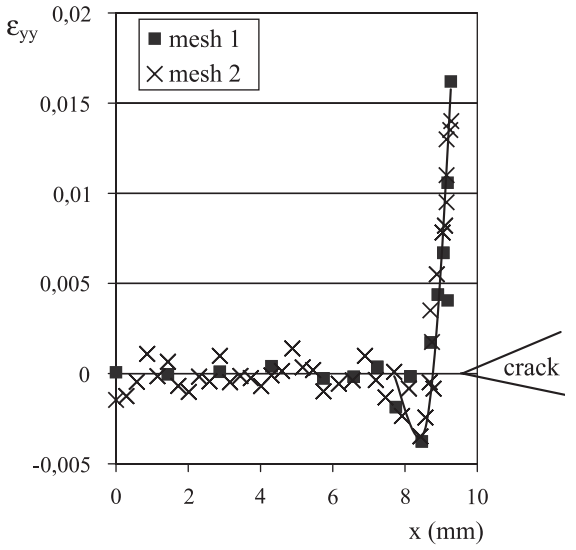

Fig. 10. Residual strains ε_{yy} created by a fatigue cycle on the TiAl alloy, measured on net section with mesh 1 and mesh 2.

Stokes [27] have measured strain contours on different thermoplastic polymers with a method based on dots tracking. The electronic speckle pattern interferometry technique has been applied by Vial-Edwards et al. [28] in order to study the neck formation in semihard copper sheets. Wattrisse et al. [17] have used the digital image correlation method for studying strain localization in steel samples, with a subwindow size of $1700\times1700\ \mu m^2$.

The optical technique used in this study has got the advantage to allow in-plane displacement measurements with a fine accuracy, and with a spatial resolution of $300\times300\ \mu m^2$. It has been applied for studying the front neck in polycarbonate tensile specimen [29]. A standard specimen (Fig. 11) is tested at room temperature, on an INSTRON tensile testing machine. Pictures of the grainy pattern are recorded in the middle of the specimen. The studied area covers $9\times4\ mm^2$.

5.2. Results

Results presented here have been obtained by correlation calculation between two consecutive pictures, corresponding to the neck front entrance in the studied zone. Because the two studied pictures are consecutive, there is no need for an adaptive mesh. Displacement measurements have been performed in 338 'points', the distance between two 'points' being equal to 360 μm. Fig. 12a presents the longitudinal strain map (ε_{xx}). The neck front is arriving in the upper side of the strain map. In this zone, measured strain values are very high, whereas out of this zone, ahead of the neck front, strain values remain homogeneous and much smaller. Strain evolution along the loading axis in the middle of the sample is plotted in Fig. 12b. Strain values vary from 12%, in the neck front, to 0.2%, in the unnecked material. This variation occurs on a 3.2-mm-long distance. In this example, the measured strain gradient is as high as $3.68\times10^{-2}\ mm^{-1}$! One can see in Fig. 12b, that, despite of this high strain gradient value, measurements have been successfully performed all along the gradient slope. And it shows the efficiency of the used digital image correlation technique for measuring simultaneously strain values from 0.2% to 12% in the same picture. Fig. 13 concerns shear strains ε_{xy}. Reliable shear strain values are difficult to obtain because of their high noise sensibility. One can see in Fig. 13a, that, as for longitudinal strains, high measured shear strain values are concentrated in the neck front. Shear strain evolution along the x-axis is plotted in Fig. 13b. The variation of the measured

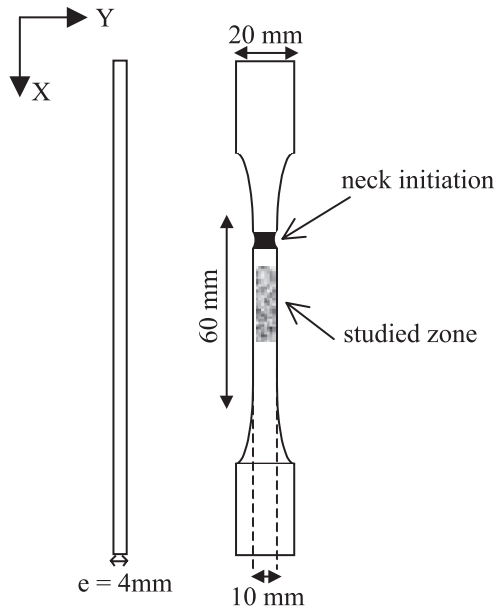

Fig. 11. Specimen geometry for tensile test on polycarbonate.

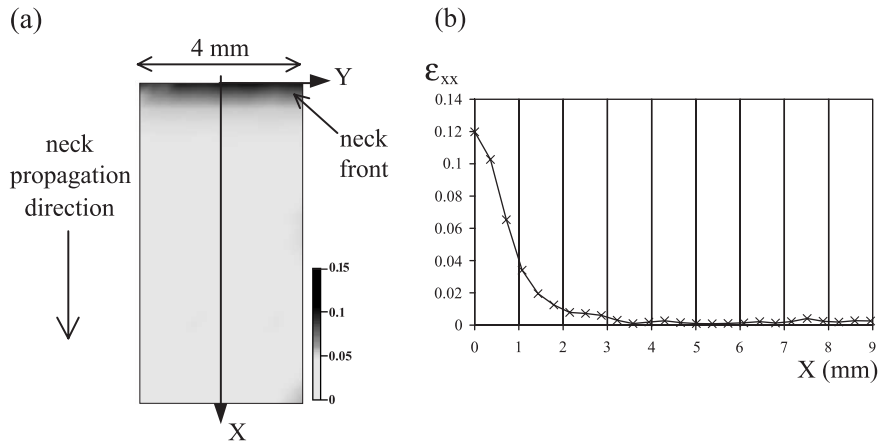

Fig. 12. Longitudinal strains ε_{xx} measured by digital image correlation technique on polycarbonate specimen: (a) strain map, (b) strain evolution along the x-axis.

shear strain values is equal to 3.2%. With this example, the used technique shows its capacity for measuring shear strain values in a severe neck front.

6. Discussion

In experimental mechanics, tested specimens often present nonhomogeneous strain distribution. It is difficult to obtain reliable measurement values in the presence of high strain gradient. Because a 'point' of measurement has necessarily a geometric dimension, the measured gradient is always more flattened than the real one. The in-plane displacement value measured at one 'point' is, in fact, the average value of displacements occurring in the considered subwindow. It is an evidence that when the subwindow size gets larger, the measured strain gradient gets more flattened. Therefore, it is necessary to use experimental techniques with high spatial resolution for studying high strain gradient. But, as it was shown in a previous work [12], the higher the spatial resolution, the worst the accuracy on displacement measurement. Thus, a compromise between both requirements has to be found. It has been also demonstrated [12] that, by using adequate experimental configuration, it is

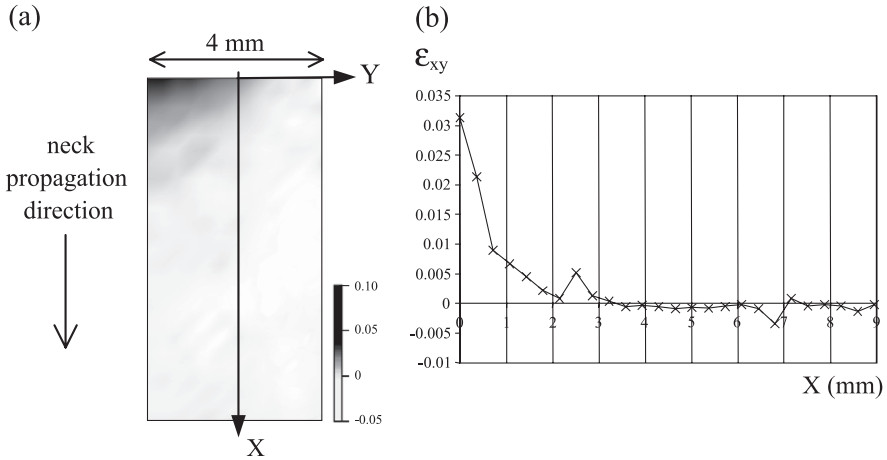

Fig. 13. Shear strains ε_{xy} measured by digital image correlation technique on polycarbonate specimen: (a) strain map, (b) strain evolution along the x-axis.

possible to measure strain values up to 12% between two consecutive pictures. That allows characterizing high strain heterogeneities.

In this study, three types of strain gradient have been studied: strain localization around a hole in a composite laminate, strain concentration at a crack tip in a TiAl alloy, and strain gradient on a polymer neck front. These three applications concern various materials: polymer, composite and metallic materials, and various types of loading: tensile test, compressive test, and fatigue test. For all these cases, the sprayed grainy pattern has shown its suitability. Different types of in-plane strain values have also been measured: residual and maximal ones, longitudinal, transverse, shear and Von Mises strains. The applied digital image correlation technique has shown, in every case, its efficiency for strain mapping and quantitative strain studying. It has been verified that the measured gradient does not depend on the tested specimen, nor on the position of the chosen mesh—provided that 'points' of measurement are numerous enough. The strain gradient values measured in these cases vary from 1.54 to 3.68×10^{-2} mm^{-1}. Thanks to the accuracy and spatial resolution performances of the used technique, it has been possible to well describe strain gradient shapes, with several points of measurement along the slope.

7. Conclusion

The aim of this paper was to study the efficiency of the digital image correlation technique for measuring in-plane displacements in the presence of high strain gradient. Strain gradient studies require to choose a good compromise between the influent parameters of this optical technique: the grain diameter, the sub-window size, the studied region size, the correlation threshold value, the distribution of the 'points' of measurement, the accuracy, and the measurable strain range. With the digital image correlation procedure that has been developed in our laboratory, the total studied area on the object surface is about 20×20 mm, and each 'point' of measurement covers an area of about 300×300 μm^2 on the object surface. Strain values up to 12% can be measured between two consecutive pictures. In this study, three types of strain gradient have been studied: strain localization around a hole in a composite laminate, strain concentration at a crack tip in a TiAl alloy, and strain gradient on a polymer neck front. These three applications concern various materials and various types of loading. Results demonstrate the efficiency of this method for strain mapping and reliable quantitative strain studying in the presence of high strain gradient values. It gives proof that this technique is able to characterize high heterogeneities in materials.

References

[1] Morimoto Y, Morimoto Jr Y, Hayashi T. Separation of isochromatics and isoclinics using Fourier transform and its accuracy. SEM Spring Conf Exp Mech 1993:1149–58.
[2] Patterson EA, Gungor S. A photoelastic study of an angle crack specimen subject to mixed mode I–III displacements. Eng Fract Mech 1997;56:767–78.
[3] Zhao B, Asundi A. Evaluating the quality of a mechanical testing system using displacement field contours. J Test Eval 1999;27:290–5.
[4] Arakawa K, Drinnon Jr RH, Kosai M, Kobayashi AS. Dynamic fracture analysis by Moiré interferometry. Exp Mech 1991;31(4):306–9.
[5] Sanford RJ. A moiré study of dynamic crack propagation in aluminum. SEM Spring Conf 1991:344–9.
[6] Rastogi PK. Principles of holographic interferometry and speckle metrology. Photomechanics. Top Appl Phys 2000;77:103–150.
[7] Yamaguchi I. Speckle displacement and decorrelation in the diffraction and image fields for small object deformation. Opt Acta 1981;28:1359–76.
[8] Joenathan C, Franze B, Haible P, Tiziani HJ. Speckle interferometry with temporal phase evaluation for measuring large-object deformation. Appl Opt 1998;37:2608–14.
[9] Asundi A. Sampled-speckle photography for measurement of deformation. Opt Lett 2000;25:218–20.
[10] Chiang FP, Wang Q, Lehman F. New developments in full field strain measurements using speckles. Nontraditional methods of sensing stress, strain and damage in materials and structures. ASTM STP 1997;1348:156–69.
[11] Lagattu F, Brillaud J, Lafarie-Frenot MC. Progress in mechanics of materials by using laser speckle method. In: Lagarde A, editor. Proceedings of IUTAM, Futuroscope, France, p. 635–42.
[12] Brillaud J, Lagattu F. Limits and possibilities of laser speckle and white light image correlation methods: theory and experiments. Appl Opt 2002;41:6603–13.
[13] Abanto-Bueno J, Lambros J. Investigation of crack growth in functionally graded materials using digital image correlation. Eng Fract Mech 2002;69:1695–711.
[14] Lyons JS, Liu J, Sutton MA. High-temperature deformation measurements using digital-image correlation. Exp Mech 1996;36:64–70.

[15] Roux S, Hild F, Berthaud Y. Correlation image velocimetry: a spectral approach. Appl Opt 2002;41(1):108–15.
[16] Chao YJ, Luo PF, Kalthoff JF. An experimental study of the deformation fields around a propagating crack tip. Exp Mech 1998;38(2):79–85.
[17] Wattrisse B, Chrysochoos A, Muracciole J-M, Némoz-Gaillard M. Analysis of strain localization during tensile tests by digital image correlation. Exp Mech 2001;41:29–39.
[18] Gonzalez J, Knauss WG. Strain inhomogeneity and discontinuous crack growth in a particulate composite. J Mech Phys Solids 1998;46(10):1981–95.
[19] Burch JM, Tokarski JMJ. Production of multi beam fringes from photographic scatters. Opt Acta 1968;15(2):101.
[20] Wisnom MR, Chang FK. Modelling of splitting and delamination in notched cross-ply laminates. Compos Sci Technol 2000;60(15):2849–56.
[21] Touchard-Lagattu F, Lafarie-Frenot MC. Damage and inelastic deformation mechanisms in thermoset and thermoplastic notched laminates. Compos Sci Technol 1996;56:557–68.
[22] Lagattu F, Lam TQ, Brillaud J, Lafarie-Frenot MC. White light speckle correlation applied to strain measurement in notched composites. In: Pusquin P, editor. Proceedings of ECCM10, Brugge, Belgium; 2002.
[23] Gloanec A-L, Bertheau D, Jouiad M, Hénaff G, Grange M, Belaygue P. Fatigue properties of a Ti–48Al–2Cr–2Nb alloy produced by casting and powder metallurgy. Third International Symposium on Gamma Titanium Aluminides (ISGTA III), TMS Annual Meeting, San Diego, CA; 2003.
[24] Lagattu F, Gloanec A-L, Henaff G, Brillaud J. Etude de la fissuration par fatigue des intermétalliques à l'aide de la technique de corrélation d'images numériques de mouchetis. Proceedings of Journée Scientifique et Technique AFM, Futuroscope, France; 2003.
[25] Bauwens-Crowet C, Ots JM, Bauwens JC. The strain-rate and temperature dependence of yield of polycarbonate in tension, tensile creep and impact tests. J Mater Sci 1974;9:1197–201.
[26] Theocaris PS, Hadjiiossiph C. Strain-analysis of neck formation and propagation in glassy polymers. Eng Fract Mech 1979;12:241–52.
[27] Nied HF, Stokes VK. Solid phase sheet forming of thermoplastics: part 2. Large deformation post-yield behavior of plastics. J Eng Mater Technol 1986;108:113–8.
[28] Vial-Edwards C, Lira I, Martinez A, Münzenmayer M. Electronic speckle pattern interferometry analysis of tensile tests of semihard copper sheets. Exp Mech 2001;41:58–62.
[29] Lagattu F, Brillaud J, Lafarie-Frenot MC. Etude par mesure de champs du front de striction dans le polycarbonate. Proceedings of 15ème Congrés Français de Mécanique, Nancy, France; 2001.